

Entropy-driven rearrangement of the water network at the hydrated amide group of the trans-formanilide-water cluster in the gas phase

Sakota, Kenji

Department of Chemistry, Graduate School of Science, Kyushu University

Shimazaki, Yuiga

Department of Chemistry, Graduate School of Science, Kyushu University

Sekiya, Hiroshi

Department of Chemistry, Graduate School of Science, Kyushu University

<https://hdl.handle.net/2324/25470>

出版情報 : Physical Chemistry Chemical Physics. 13 (14), pp.6411-6415, 2011-03-03. RSC Publishing

バージョン :

権利関係 : (C) 2011 the Owner Societies



Entropy-driven rearrangement of the water network at the hydrated amide
group of the *trans*-formanilide-water cluster in the gas phase

Kenji Sakota, Yuiga Shimazaki and Hiroshi Sekiya*

Department of Chemistry, Faculty of Sciences, and Department of Molecular
Chemistry, Graduate School of Science, Kyushu University, 6-10-1 Hakozaki,
Higashi-ku, Fukuoka 812-8581, Japan

* E-mail: sekiya@chem.kyushu-univ.jp

Abstract

Photo-ionization induced rearrangement of a water network in *trans*-formanilide 1:4 cluster, FA-(H₂O)₄, has been investigated by using IR-photodissociation spectroscopy and quantum chemical calculations. The IR spectrum of FA-(H₂O)₄ in the S₀ state shows that the observed cluster has a cyclic hydrogen-bonded structure where the CO group and the NH group of FA are bridged with four water molecules, consistent with the reported structure [E. G. Robertson, *Chem. Phys. Lett.* 2000, **325**, 299]. However, the corresponding cyclic hydrogen-bonded structure in the D₀ state of [FA-(H₂O)₄]⁺ is a minor product arising from photoionization via the S₁-S₀ origin of FA-(H₂O)₄. The dominant product has an extended H-bonded structure, where the intermolecular hydrogen bond between the hydrogen of the OH group of a water molecule and the CO group is dissociated. This is the first observation of a photoionization-induced rearrangement of water network in [FA-(H₂O)₄]⁺. Through DFT calculations, we conclude that the rearrangement occurs due to the entropic effects.

Over the past few decades, laser spectroscopy has proved to be a powerful tool for investigating the molecular structures and their dynamics in both the condensed phase and the gas phase.¹ Recently, biological molecules such as proteins, DNA bases, and amino acids have been attractive targets for laser spectroscopy, with the aim of understanding their intriguing properties at the molecular level.²⁻⁴ The laser spectroscopy of biologically-relevant molecules in the gas phase has also advanced due to the invention of ingenious vaporization techniques such as electrospray ionization and matrix-assisted laser desorption/ionization.⁵ The hydrogen-bonding (H-bonding) interaction has been widely studied due to its central role in chemistry and biology.⁶ The hydration structures in biological systems are one of the most important factors in controlling their structures and functions. The hydrophilic groups in biological molecules form H-bonds with surrounding water molecules. The H-bonds constrain the structures of biological molecules when the hydrophilic groups preferentially make contact with the aqueous phase. In addition, the hydrophobic interaction causes the rearrangements of hydration structures, which minimizes the contact area between the hydrophobic groups and the water molecules. From a thermodynamic point of view, the hydrophilic and hydrophobic interactions can be understood as a consequence of a subtle balance between enthalpy and entropy.^{7,8}

In gas-phase studies, the supersonic jet expansion technique has been successfully applied to investigate the characteristic features of H-bonds.⁹⁻¹³ However, in general, the temperature of jet-cooled H-bonded clusters is too low to observe the entropic effects. The H-bonded clusters with large internal energies are ideal model systems to investigate such entropic effects, because detailed analyses are possible for limited-size clusters by combining spectroscopic measurements with theoretical studies. However, the role of entropic effects on H-bonded networks has not been clarified due to a lack of experimental studies on the rearrangements of H-bonded networks in the gas phase

in spite of the importance of this role in the dynamics.¹⁴

In this communication, we report the IR photodissociation (IRPD) spectrum of the *trans*-formanilide (FA)-water 1:4 cluster cation, $[\text{FA}-(\text{H}_2\text{O})_4]^+$, which was formed in the cationic ground (D_0) state by photoionization of $\text{FA}-(\text{H}_2\text{O})_4$. FA has an amide group, which is one of the most important functional groups that constitute the backbone of proteins. The geometries and vibrational structures of FA and hydrated FA were investigated by resonant two-photon ionization (R2PI) spectroscopy, IR-dip spectroscopy, and ZEKE (Zero kinetic energy) photoelectron spectroscopy.¹⁵⁻²⁰ However, little is known about the the dynamics of these molecules. We report here for the first time the observation of an entropy-driven rearrangement of the water network at the amide group of $[\text{FA}-(\text{H}_2\text{O})_4]^+$. We discuss its mechanism by combining the experimental results with theoretical calculations.

The experimental setup was described in detail elsewhere.²¹ Briefly, FA was introduced in a stainless steel tube. The sample was heated to 373 K using a coiled heater, and the vaporized molecules were expanded into a vacuum chamber with Ne as a carrier gas, which passed through a reservoir containing water. A differentially pumped linear time-of-flight mass spectrometer was used to measure the R2PI, IR-dip, and IRPD spectra. For the R2PI experiment, a frequency-doubled dye-laser (Sirah Cobra stretch) pumped by the second harmonic of an Nd^{3+} :YAG laser (Spectra Physics INDI, 20 Hz) was used as a UV source. Typical UV laser power was ~ 300 $\mu\text{J}/\text{pulse}$. An optical parametric converter (LaserVision) pumped by an injection-seeded Nd^{3+} :YAG laser (Continuum Powerlite Precision II 8000, 10 Hz) was used as an IR source. Typical IR laser power was 1~2 mJ/pulse. For the IR-dip spectroscopy in the S_0 state, IR irradiation proceeded UV irradiation by 50 ns. When the IR photon was resonant with the vibrational transition of $[\text{FA}-(\text{H}_2\text{O})_4]$ in S_0 , the intensity of signal from the parent ion, $[\text{FA}-(\text{H}_2\text{O})_4]^+$, was reduced. Thus, we obtained the IR spectrum

in S_0 as the depletion of the parent mass signal. For the IRPD spectroscopy in the D_0 state, the cluster ion was produced by the R2PI process, followed by IR irradiation. The time delay between the UV and IR pulses was 800 ns. When the IR photon energy was resonant with the vibrational transition of the cluster cation, fragmentation occurs, causing an enhancement of the signals from the fragment species ($[\text{FA}-(\text{H}_2\text{O})_3]^+$ and $[\text{FA}-(\text{H}_2\text{O})_2]^+$). We obtained the IRPD spectrum in D_0 by monitoring the enhancements of the fragment species. As the intensities of the fragment species of $[\text{FA}-(\text{H}_2\text{O})_1]^+$ were quite low, we did not monitor their intensities by IRPD spectroscopy.

Density functional theory (DFT) calculations were performed at the wB97XD/6-311++G(3df,3pd) level of theory to obtain stable structures, harmonic vibrational frequencies, and IR intensities for $\text{FA}-(\text{H}_2\text{O})_4$ and $[\text{FA}-(\text{H}_2\text{O})_4]^+$. The calculated harmonic vibrational frequencies were scaled by 0.9439. The relative stabilization energies for the isomers of $[\text{FA}-(\text{H}_2\text{O})_4]^+$ were obtained by single-point energy calculations at the ROCCSD(T)//6-311++G(2df,2pd)/6-311G(d,p) level of theory, and the stable structures were obtained at the wB97XD/6-311++G(3df,3pd) level of theory, where the 6-311G(d,p) and 6-311++G(2df, 2pd) basis sets were used for the aromatic ring moiety and the other moieties of $[\text{FA}-(\text{H}_2\text{O})_4]^+$, respectively. The zero point energy corrections were performed by using calculated vibrational frequencies obtained at the uwB97XD/6-311++G(3df,3pd) level. All calculations were performed using the GAUSSIAN 09 program package.²²

Fig. 1(a) shows the (1+1) R2PI spectrum of FA, which is essentially the same as that reported previously.^{15,16} A strong vibronic band is observed at 36005 cm^{-1} , which is assigned to the S_1 - S_0 origin of FA. Fig. 1(b) shows the (1+1) R2PI spectrum of $\text{FA}-(\text{H}_2\text{O})_4$. In the previous study, the vibronic band at 35992 cm^{-1} was assigned to the S_1 - S_0 origin of $\text{FA}-(\text{H}_2\text{O})_4$, which is red-shifted by 13 cm^{-1} from that of FA.¹⁷ In Fig. 1(b), weak vibronic transitions are observed in the vicinity of the origin band,

which can be attributed to the intermolecular vibrations of FA-(H₂O)₄.

Fig. 2 shows the IR-dip spectrum of FA-(H₂O)₄ in the S₀ state. This spectrum is essentially the same as that reported previously.¹⁷ The stick spectrum shown in the lower panel of Fig. 2 is a theoretical IR spectrum of FA-(H₂O)₄ calculated at the wB97XD/6-311++G(3pd,3df) level of theory. The inset in Fig. 2 indicates the calculated stable structure. In the previous study, based on the (1+1) R2PI spectra measured by monitoring the mass channels of [FA-(H₂O)_n]⁺ (n=2-5) and the IR-dip spectrum, the observed species in Fig. 2 was assigned to the isomer that has a cyclic H-bonded structure, where the NH group and the CO group of FA are bridged with four water molecules as shown in Fig. 2.¹⁷ In the theoretical IR spectrum, five strong transitions are predicted in the region from ~3200 cm⁻¹ to ~3400 cm⁻¹, which correspond to the H-bonded NH and OH stretching vibrations, although more than five vibrational transitions are observed in the same wavenumber region in the IR-dip spectrum. The contributions of larger clusters to the IR-dip spectrum in Fig. 2 is ruled out in Ref. 17 based on the position of the origin band in the R2PI spectrum and its fragmentation pattern. In addition, the origin band of FA-(H₂O)₄ in Fig. 1 is sharp enough to eliminate the contributions of the bands of another isomers to the IR-dip spectrum in Fig. 2. According to Ref. 17 the observation of the extra vibrational transitions is attributed to a Fermi resonance of the NH and/or OH stretch fundamentals and the 2v₂ overtones in one or more water molecules.

Fig. 3(a) shows the IRPD spectrum in D₀ of [FA-(H₂O)₄]⁺. Fig. 3(b)-3(g) show theoretical IR spectra of the [FA-(H₂O)₄]⁺ isomers calculated at the uwB97XD/6-311++G(3df,3pd) level of theory. The calculated stable structures are indicated in Fig. 4. Strong vibrational transitions predicted below 2900 cm⁻¹ correspond to the H-bonded NH stretching vibrations. In Fig. 3(a), a broad vibrational transition centered at ~2600 cm⁻¹ is observed. The theoretical IR spectra in Fig.

3(b)-3(d) well explain the vibrational transition around 2600 cm^{-1} in Fig. 3(a). In addition, a broad vibrational transition, whose center is located at $\sim 3300\text{ cm}^{-1}$, is detected in Fig. 3(a). This transition is well reproduced in the calculated spectrum in Fig. 3(b) or 3(c). In Fig. 3(a), a strong vibrational transition is observed at $\sim 3480\text{ cm}^{-1}$, which is also well reproduced in the calculated spectrum in Fig. 3(b) or 3(c). Thus, we concluded that the observed species that provides Fig. 3(a) corresponds to the isomers that show the spectrum in Fig. 3(b) and/or 3(c). A difference in the structure of isomers between (i) and (ii) in Fig. 4, which provide the spectra in Fig. 3(b) and (c), respectively, is only the position of the water located at the end of water network. It is difficult to distinguish the IR spectrum of isomer (i) from that of isomer (ii) due to very similar patterns. We cannot exclude the possibility that the transitions of the other isomers in Fig. 3(d)-(g) overlap with those in Fig. 3(b) and (c), since the IRPD spectrum in Fig. 3(a) is very broad. In order to examine the overlap with the transitions of another isomers the theoretical IR spectrum was convoluted with the bandwidths of each vibrational transitions indicated by a solid line. The bandwidths convoluted for the theoretical IR spectra in Fig. 3(b) and 3(c) are adopted from those obtained from experimentally. The solid line in Fig. 3(b) and 3(c) well reproduces the experimental one. Therefore, we conclude that the transitions that appear in Fig. 3(b) and/or 3(c) are mainly contributors to the observed IRPD spectrum in Fig. 3(a), i.e., the dominant products are isomer (i) and/or isomer (ii).

In the S_0 state, FA-(H₂O)₄ has a cyclic H-bonded structure (Fig. 2). When the cyclic H-bonded FA-(H₂O)₄ is ionized via the S_1 - S_0 origin of FA-(H₂O)₄, isomer (iv) in Fig. 4 having a similar structure in the S_0 state, should be observed, because the vertical transition occurs in the photoionization process. However, in Fig. 3(a), isomer (i) and/or (ii) were observed as the dominant product. This observation explicitly indicates that the H-bonded network of water molecules in [FA-(H₂O)₄]⁺

rearranges from the cyclic hydrogen-bonded structure (iv) to the extended H-bonded structure of isomer (i) and/or (ii) in the D_0 state. A schematic energy diagram is illustrated in Fig. 5 to show the photo ionization-induced rearrangement of $[\text{FA}-(\text{H}_2\text{O})_4]^+$.

In Fig. 4, the zero-point energy corrected relative stabilization energies at the ROCCSD(T)//6-311++G(2df, 2pd)/6-311G(d,p) level of theory are indicated for each isomers. The most stable isomer of $[\text{FA}-(\text{H}_2\text{O})_4]^+$ is isomer (iv), where four water molecules form a cyclic structure between the NH group and the CO group of FA^+ . In Fig. 3(a), however, isomers (i) and/or (ii) are observed, although isomers (i) and (ii) are unstable by 0.59 and 0.71 kcal/mol, respectively, as compared with the most stable isomer (iv). Thus, the relative stabilization energies of each isomers cannot well explain the rearrangement of the H-bonded network of water molecules in $[\text{FA}-(\text{H}_2\text{O})_4]^+$.

Fig. 6 shows the logarithmic curves of the vibrational density of states (vDOS) for each structural isomers in the D_0 state as a function of the excess internal vibrational energy of isomer (iv). The vDOSs of each isomers are calculated by the Beyer-Swinehart direct counting algorithm.²³ The scaled harmonic vibrational frequencies obtained at the uwB97XD/6-311++G(3df, 3pd) level of theory are used to calculate vDOSs. We assume that the excess internal energy of $[\text{FA}-(\text{H}_2\text{O})_4]^+$ is dominated by the internal vibrational energy in the D_0 state, because $\text{FA}-(\text{H}_2\text{O})_4$ is produced under the supersonic jet-cooled conditions. Therefore the internal rotational energy of $[\text{FA}-(\text{H}_2\text{O})_4]^+$ is likely quite small even after photoionization. When chemical equilibrium is achieved at internal energy E in the D_0 state of $[\text{FA}-(\text{H}_2\text{O})_4]^+$, the relative abundances of the isomers, i.e. the equilibrium constant, can be elucidated by the ratio of their vDOSs,

$$K(E) = \frac{W_X(E)}{W_Y(E)} \quad (1)$$

where $K(E)$ is the equilibrium constant, and $W_X(E)$ and $W_Y(E)$ are the equilibrium constant, and the vDOSs of isomers (X) and (Y) respectively at internal energy E . The (TD)DFT calculations at the wB97XD/6-311++G(3df,3pd) level of theory predict that $[\text{FA}-(\text{H}_2\text{O})_4]^+$ has an internal energy of 9.44 kcal/mol in the D_0 state for the vertical transition from the S_1 state to the D_0 state. In Fig. 6, the position of the vertical transition is indicated by an arrow. In this wavenumber region, the vDOSs of isomers (i) and (ii) indicated by the red solid and broken lines, respectively, are about three orders of magnitude larger than that of isomer (iv). It should be noted that the internal energy of $[\text{FA}-(\text{H}_2\text{O})_4]^+$ in the D_0 state shows a distribution corresponding to the Franck-Condon overlaps between the S_1 and the D_0 state. But, the vDOSs of isomers (i) and (ii) are larger than those of the other isomers in the whole wavenumber region in Fig. 6. Thus, based on the vDOSs of each isomer in Fig. 6, isomers (i) and (ii) show the largest population for $[\text{FA}-(\text{H}_2\text{O})_4]^+$, which is consistent with the experimental result. It is worth noting that the low-wavenumber intermolecular vibrations make large contributions to the vDOSs of each isomer. For example, the torsional vibrations usually show large anharmonicities, leading to a reduction of their wavenumbers.^{24,25} Therefore, the vDOSs shown in Fig. 6 are the lower limits of the vDOSs. In this work, we did not take into account the effect of anharmonicity on the vDOS of the isomers explicitly. However, it is clear that the vDOSs of isomers (i) and (ii) in Fig. 6 are much larger than those of the other isomers. This result will not change even if the anharmonicities are accounted for.

Let us assume the principle of the equal weight for each vibrational states at the internal energy E , the probability that one vibrational state is populated among the total vibrational states in the D_0 state can be written by

$$p_i = \frac{1}{\sum_j W_j(E)} = \frac{1}{W_{total}(E)} \quad (2)$$

where p_i is the probability mentioned above, $W_j(E)$ is the vDOS for isomer (j), and $W_{total}(E)$ is the sum of $W_j(E)$ for isomer (j). From this definition, the total vibrational entropy in the chemical equilibrium can be defined by the Gibbs entropy,

$$S(E) = -k_B \sum_i p_i \ln p_i \quad (3)$$

where $S(E)$ is the total vibrational entropy at the internal energy E , and k_B is the Boltzmann constant. By using equation (2) and (3), the vibrational entropy of isomer (j) can be written as

$$S_j(E) = k_B p_j \ln W_{total}(E) \quad (4)$$

where

$$p_j = \frac{W_j(E)}{W_{total}(E)} \quad (5)$$

$W_j(E)$ is the vDOS of isomer (j) at the internal energy E . By using equation (1) and (4), the equilibrium constant can be written as

$$K(E) = \frac{S_X(E)}{S_Y(E)} \quad (6)$$

Equation (6) indicates that the relative abundances of each structural isomers of $[\text{FA}-(\text{H}_2\text{O})_4]^+$ can be elucidated by determining their vibrational entropies, i.e., the population at internal energy E increases as the vibrational entropy increases. Therefore, from a thermodynamic point of view, the rearrangement of the H-bonded network in the amide group of $[\text{FA}-(\text{H}_2\text{O})_4]^+$ observed in this study can be considered as an entropy-driven phenomenon, i.e., the driving force of the reaction is entropy. This is a manifestation of the second law of thermodynamics. It should be noted that the rearrangement of the hydration structure of monohydrated aromatic molecules were

reported previously.²⁶⁻²⁸ Recently, we also found water migration between the CO group and the NH group in the amide group of the *trans*-acetanilide-water 1:1 cluster cation.²⁹ Our previous study, however, did not focus on the entropic effects as the driving force of the rearrangement of the hydration structure.

In protein folding, the rearrangements of the hydration structures around the amide groups play an important role, because dehydration of water molecules from the amide groups followed by the formations of H-bonds between the amide groups is an important step in allowing proteins to fold their proper structures. The change of the free energy, which consists of the enthalpy and entropy terms, governs the folding process. We have shown that the rearrangement of hydration structures in the amide group proceeds by an entropic effect. This finding implies that the entropy change caused by the rearrangement of hydration structures around amide groups is one of the origins of the change of the free energy in the folding process at the molecular level. Thus, we have to take into account of the contribution of environmental water molecules as well as biological molecules to determine the change in the free energy.

In summary, this is the first observation of the rearrangement of the H-bonded network of water molecules in the amide group of $[\text{FA}-(\text{H}_2\text{O})_4]^+$ achieved using IRPD spectroscopy. The experimental results indicate that the H-bonded network of $[\text{FA}-(\text{H}_2\text{O})_4]^+$ rearranges from the cyclic H-bonded structure to the extended H-bonded structure in photoionization. Based on the calculations of the vibrational density of states of each isomer of $[\text{FA}-(\text{H}_2\text{O})_4]^+$, the rearrangement of the H-bonded network observed in this study can be ascribed to an entropy-driven phenomenon.

This work was partly supported by the Grant-in Aid for Scientific Research B (20350011), the Grant-in-Aid for Scientific Research in Priority Area (477) “Molecular Science for Supra Functional Systems – Development of Advanced Methods for Exploring elementary Processes” (19056005) from the Japanese Ministry of Education,

Sports, Science and Technology (MEXT). The computations were carried out by using the computer facilities at Research Institute for Information Technology, Kyushu University.

References

- 1 W. Demtröder, *Laser spectroscopy: Vol. 1 and Vol. 2*, Springer, 2008.
- 2 J. T. Pelton and L. R. McLean, *Anal. Biochem.* 2000, **277**, 167.
- 3 E. Nir, K. Kleineremanns and M. S. de Vries, *Nature* 2000, **408**, 949.
- 4 E. G. Robertson and J. P. Simons, *Phys. Chem. Chem. Phys.* 2001, **3**, 1.
- 5 T. R. Rizzo, J. A. Stearns and O. V. Boyarkin, *Int. Rev. Phys. Chem.* 2009, **28**, 481, and references therein.
- 6 G. A. Jeffrey and W. Saenger, *Hydrogen bonding in biological structures*, Springer, Verlag, 1991.
- 7 W. Kauzmann, *Adv. Protein. Chem.* 1959, **14**, 1.
- 8 N. T. Southall, K. A. Dill and A. D. J. Haymet, *J. Phys. Chem. B* 2002, **106**, 521.
- 9 T. S. Zwier, *Annu. Rev. Phys. Chem.* 1997, **47**, 205.
- 10 T. Ebata, A. Fujii and N. Mikami, *Int. Rev. Phys. Chem.* 1998, **17**, 331.
- 11 B. Brutschy, *Chem. Rev.* 2000, **100**, 3999.
- 12 H. Sekiya and K. Sakota, *J. Photochem. Photobiol. C* 2008, **9**, 81.
- 13 Y. Matsuda, N. Mikami and A. Fujii, *Phys. Chem. Chem. Phys.* 2009, **11**, 1279.
- 14 V. A. Shubert, E. E. Baquero, J. R. Clarkson, W. H. James, J. A. Turk, A. A. Hare, K. Worrel, M. A. Lipton, D. P. Schofield, K. D. Jordan and T. S. Zwier, *J. Chem. Phys.* 2007, **127**, 234315.
- 15 V. P. Manea, K. J. Wilson and J. R. Cable, *J. Am. Chem. Soc.* 1997, **119**, 2033.
- 16 J. A. Dickinson, M. R. Hockridge, E. G. Robertson and J. P. Simons, *J. Phys. Chem. A* 1999, **103**, 6938.
- 17 E. G. Robertson, *Chem. Phys. Lett.* 2000, **325**, 299.
- 18 M. Mons, I. Dimicoli, B. Tardivel, F. Piuze, E. G. Robertson and J. P. Simons, *J. Phys. Chem. A* 2001, **105**, 969.
- 19 S. Ullrich, X. Tong, G. Tarczay, C. E. H. Dessent and K. Muller-Dethlefs, *Phys.*

Chem. Chem. Phys. 2002, **4**, 2897.

20 M. Miyazaki, J. Saikawa, H. Ishizaki, T. Taira and M. Fujii, *Phys. Chem. Chem. Phys.* 2009, **11**, 6098.

21 Y. Kageura, K. Sakota and H. Sekiya, *J. Phys. Chem. A* 2009, **113**, 6880.

22 Gaussian 09, Revision **A.1**, M. J. Frisch, G. W. Trucks, H. B. Schlegel, G. E. Scuseria, M. A. Robb, J. R. Cheeseman, G. Scalmani, V. Barone, B. Mennucci, G. A. Petersson, H. Nakatsuji, M. Caricato, X. Li, H. P. Hratchian, A. F. Izmaylov, J. Bloino, G. Zheng, J. L. Sonnenberg, M. Hada, M. Ehara, K. Toyota, R. Fukuda, J. Hasegawa, M. Ishida, T. Nakajima, Y. Honda, O. Kitao, H. Nakai, T. Vreven, J. A. Montgomery, Jr., J. E. Peralta, F. Ogliaro, M. Bearpark, J. J. Heyd, E. Brothers, K. N. Kudin, V. N. Staroverov, R. Kobayashi, J. Normand, K. Raghavachari, A. Rendell, J. C. Burant, S. S. Iyengar, J. Tomasi, M. Cossi, N. Rega, J. M. Millam, M. Klene, J. E. Knox, J. B. Cross, V. Bakken, C. Adamo, J. Jaramillo, R. Gomperts, R. E. Stratmann, O. Yazyev, A. J. Austin, R. Cammi, C. Pomelli, J. W. Ochterski, R. L. Martin, K. Morokuma, V. G. Zakrzewski, G. A. Voth, P. Salvador, J. J. Dannenberg, S. Dapprich, A. D. Daniels, Ö. Farkas, J. B. Foresman, J. V. Ortiz, J. Cioslowski, and D. J. Fox, Gaussian, Inc., Wallingford CT, 2009.

23 S. E. Stein and B. S. Rabinovitch, *J. Chem. Phys.* 1973, **58**, 2438.

24 K. D. Kolenbrander, C. E. Dykstra, J. M. Lisy, *J. Chem. Phys.* 1988, **88**, 5995.

25 T. Haino, K. Fukuta, H. Iwamoto and S. Iwata, *Chem. Eur. J.* 2009, **15**, 13286.

26 M. Gerhards, A. Jansen, C. Unterberg and A. Gerlach, *J. Chem. Phys.* 2005, **123**, 074320.

27 J. R. Clarkson, E. Baquero, V. A. Shubert, E. M. Myshakin, K. D. Jordan and T. S. Zwier, *Science* 2005, **307**, 1443.

28 H. M. Kim, K. Y. Han, J. Park, G. S. Kim and S. K. Kim, *J. Chem. Phys.* 2008, **128**, 041104.

29 K. Sakota, S. Harada, Y. Shimazaki and H. Sekiya, To be published.

Figure captions

Fig. 1 (a) (1+1) R2PI spectrum of FA. The S_1 - S_0 origin band is observed at 36005 cm^{-1} . (b) (1+1) R2PI spectrum obtained by monitoring the $[\text{FA}-(\text{H}_2\text{O})_4]^+$ mass channel. The S_1 - S_0 origin band of $\text{FA}-(\text{H}_2\text{O})_4$ is observed at 35992 cm^{-1} , which is red-shifted by 13 cm^{-1} from that of FA.

Fig. 2 IR-dip spectrum of $\text{FA}-(\text{H}_2\text{O})_4$ in the S_0 state obtained by probing the origin band at 35992 cm^{-1} . The theoretical IR spectrum calculated at wB97XD/6-311++G(3df, 3pd) is shown in the bottom. The harmonic vibrational frequencies are scaled by 0.9439. The inset indicates the calculated stable structure of $\text{FA}-(\text{H}_2\text{O})_4$.

Fig. 3 (a) IRPD spectrum of $[\text{FA}-(\text{H}_2\text{O})_4]^+$ obtained by monitoring the $[\text{FA}-(\text{H}_2\text{O})_n]^+$ ($n=2,3$) mass channels. The intensity of IRPD spectrum is normalized by IR intensity. (b)-(g) Theoretical IR spectra calculated at the uwB97XD/6-311++G(3df, 3pd) level of theory. The calculated stable structures that provide theoretical IR spectra are shown in Fig. 4. The harmonic vibrational frequencies are scaled by 0.9439. The solid curves in (b) are the theoretical IR spectra convoluted with bandwidths of 250 cm^{-1} for the vibrational bands at 2587 and 3299 cm^{-1} , 100 cm^{-1} for the bands at 3440 and 3462 cm^{-1} , and 15 cm^{-1} for the other vibrational bands, respectively. The bandwidths are adopted from the experimental IRPD spectrum. For the solid curve in (c), convolution was performed with the same bandwidths.

Fig. 4 The stable structures calculated at the uwB97XD/6-311++G(3df, 3pd) level of theory. The relative stabilization energies are indicated, which are obtained by the single-point energy calculations at the ROCCSD(T)//6-311++G(2df,2pd)/6-311G(d,p) level of theory for the stable structures obtained at the uwB97XD/6-311++G(3df,3pd) level

. The zero-point energy corrections are performed by using the calculated vibrational frequencies obtained at uwB97XD/6-311++G(3df,3pd). The numbers of each isomers (i)-(vi) correspond to those shown in Fig. 3.

Fig. 5 A schematic energy diagram of the rearrangement of the H-bonded network in $[\text{FA}-(\text{H}_2\text{O})_4]^+$. The extended H-bonded structure on the right-hand side of the figure is unstable by 0.59 kcal/mol as compared with the cyclic-H-bonded structure on the left-side of the figure. The detailed rearrangement path and the barrier height along the path have not been obtained.

Fig. 6 The logarithmic curves of the vibrational density of states (vDOS) for each isomers as a function of the internal energy of the most stable isomer (iv). The red solid and broken lines, the black solid and broken lines, the green solid line, and the blue solid line correspond to vDOSs of isomers (i), (ii), (iii), (v), (vi), and (iv), respectively. The position of an arrow in the figure shows the position where the vertical transition from the S_1 to the D_0 state occurs.

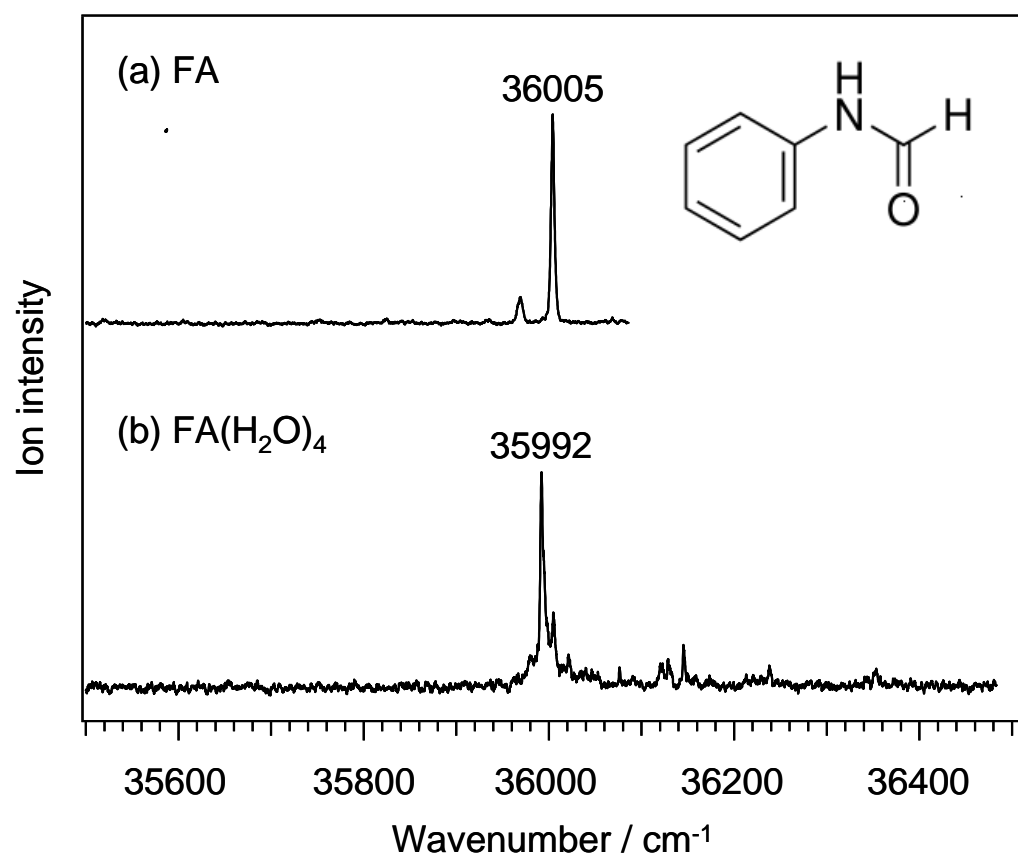


Fig. 1

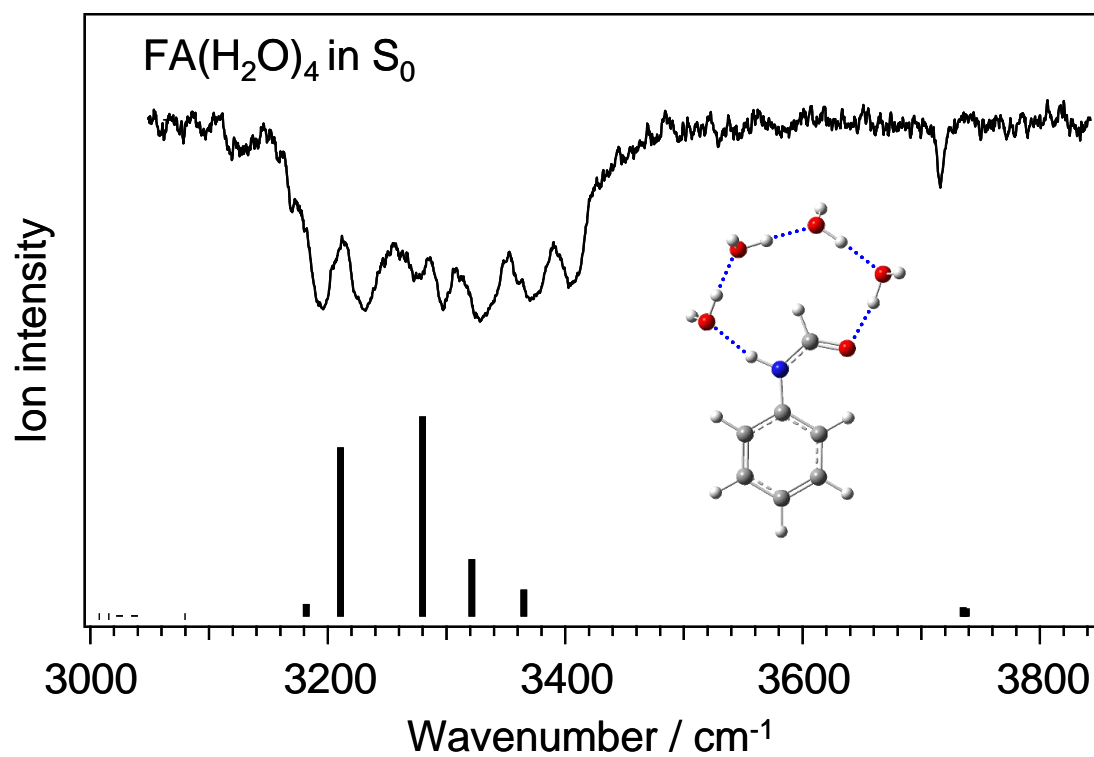


Fig. 2

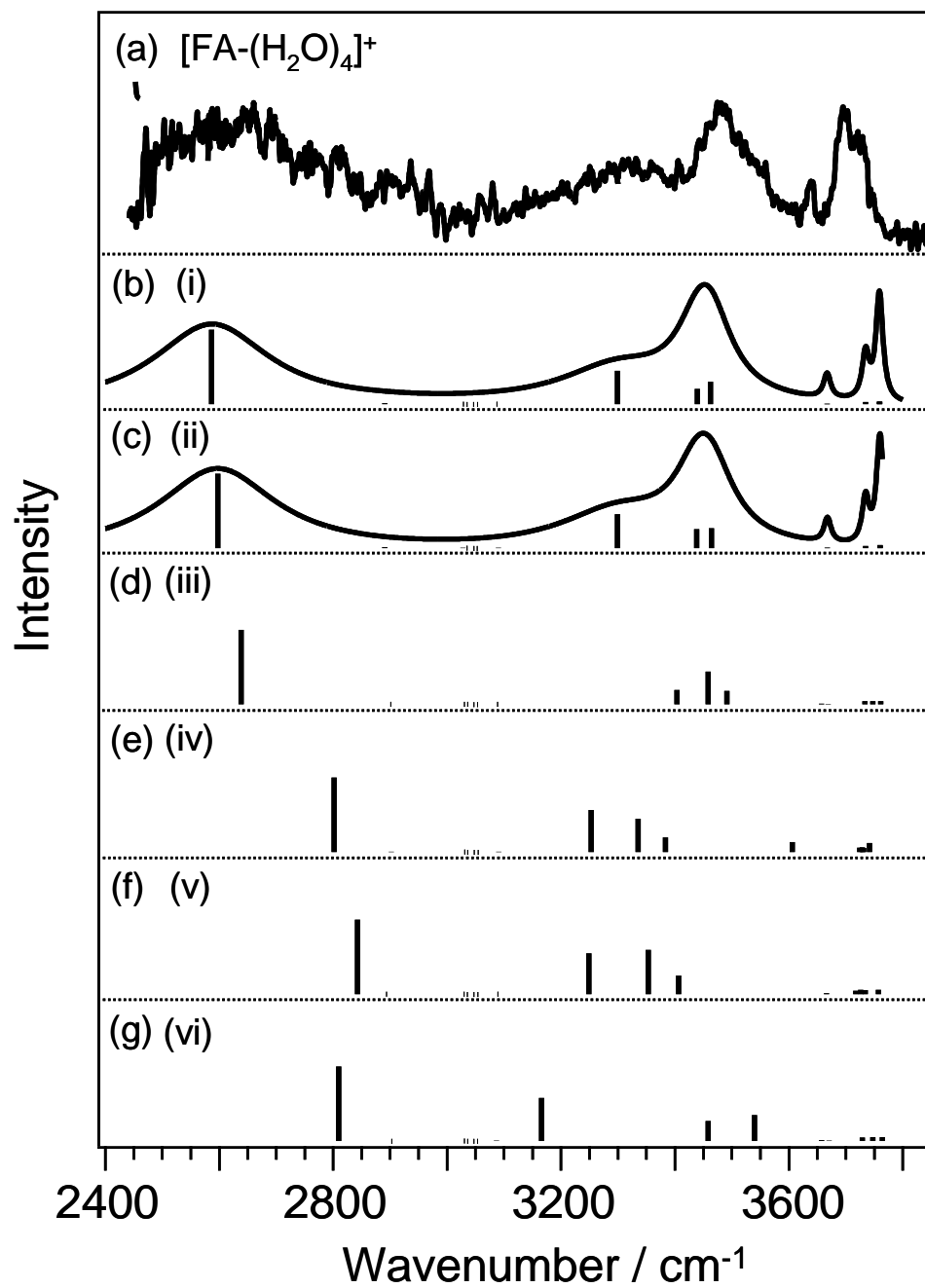


Fig. 3

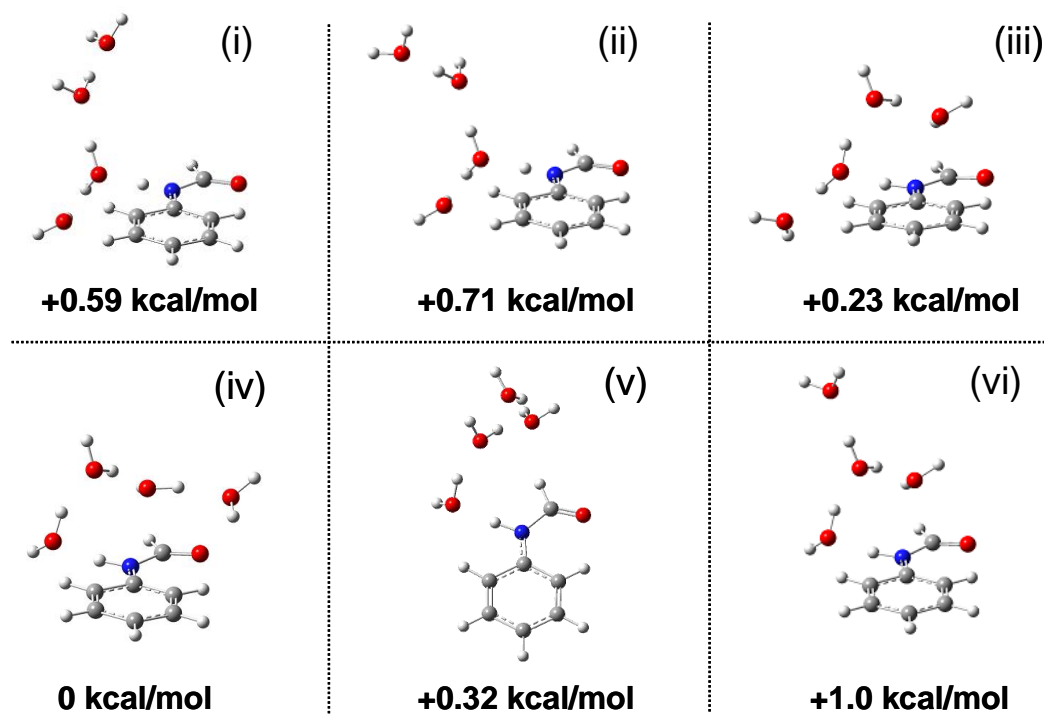


Fig. 4

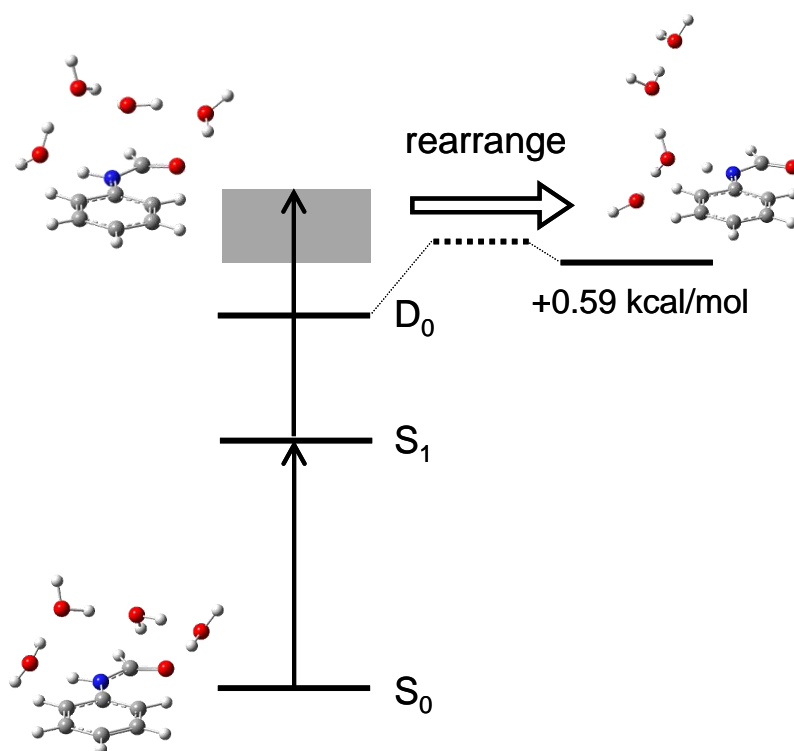


Fig. 5

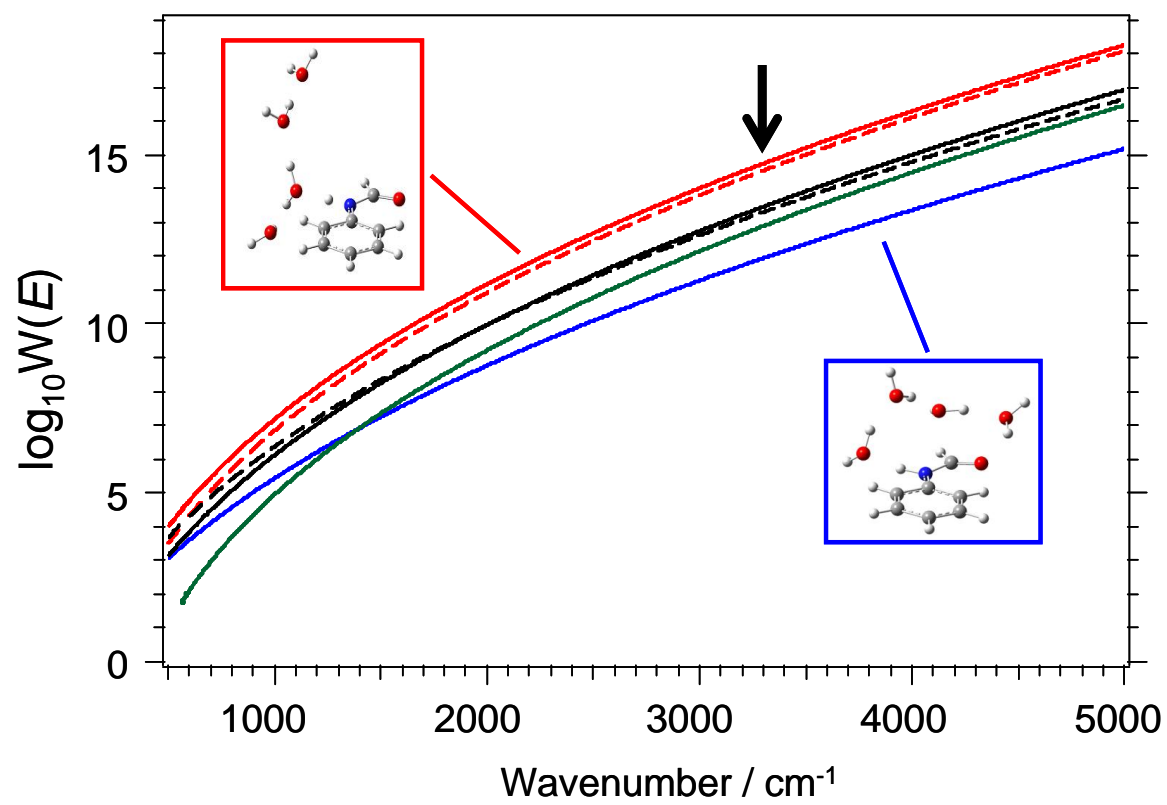


Fig. 6

Graphical Abstract

